International Journal of Nanomedicine

Dovepress
open access to scientific and medical research

Open Access Full Text Article

ORIGINAL RESEARCH

Effects of adsorbed and templated nanosilver in mesoporous calcium-silicate nanoparticles on inhibition of bacteria colonization of dentin

This article was published in the following Dove Press journal:
International Journal of Nanomedicine
12 November 2014
Number of times this article has been viewed

Wei Fan[1,*]
Daming Wu[1,*]
Franklin R Tay[2]
Tengjiao Ma[1]
Yujie Wu[1]
Bing Fan[1]

[1]The State Key Laboratory Breeding Base of Basic Science of Stomatology (Hubei-MOST) and Key Laboratory of Oral Biomedicine Ministry of Education, School and Hospital of Stomatology, Wuhan University, Wuhan, People's Republic of China; [2]Department of Endodontics, Georgia Regents University, Augusta, Georgia, USA

*These authors contributed equally to this work

Abstract: Mesoporous calcium-silicate nanoparticles (MCSNs) are advanced biomaterials for controlled drug delivery and mineralization induction. Nanosilver-incorporated MCSNs (Ag-MCSNs) were prepared in the present study using both the adsorption and template methods. Both versions of Ag-MCSNs showed characteristic morphology of mesoporous materials and exhibited sustained release of ions over time. In antibacterial testing against planktonic *Enterococcus faecalis*, Ag-MCSNs showed significantly better antibacterial effects when compared with MCSNs ($P<0.05$). The Ag-MCSNs aggregated on the dentin surface of root canal walls and infiltrated into dentinal tubules after ultrasound activation, significantly inhibiting the adherence and colonization of *E. faecalis* on dentin ($P<0.05$). Despite this, Ag-MCSNs with templated nanosilver showed much lower cytotoxicity than Ag-MCSNs with adsorbed nanosilver ($P<0.05$). The results of the present study indicated that nanosilver could be incorporated into MCSNs using the template method. The templated nanosilver could release silver ions and inhibit the growth and colonization of *E. faecalis* both in the planktonic form and as biofilms on dentin surfaces as absorbed nanosilver. Templated Ag-MCSNs may be developed into a new intracanal disinfectant for root canal disinfection due to their antibacterial ability and low cytotoxicity, and as controlled release devices for other bioactive molecules to produce multifunctional biomaterials.

Keywords: antibacterial effect, mesoporosity, root canal, silver

Introduction

An essential aspect of clinical biomaterials application is infection prevention and control.[1] Antibacterial biomaterials are useful for the treatment of hard tissue-related infectious diseases.[2,3] For example, persistent apical periodontitis and bone loss around the root apex after root canal treatment is caused by reinfection and bacteria colonization of the canal wall dentin.[4,5] Bacteria in root canals adhere to canal wall dentin and penetrate dentinal tubules up to a depth of 200–1,500 μm.[6,7] Thus, antibacterial materials designed for use in root canals should be capable of adhering to dentin surfaces, infiltrating into the dentinal tubules,[8] and promoting remineralization of dentin.[9]

Nanoparticles infiltrate fine anatomical structures much more easily than materials in the micrometer scale.[8,10] Because of their high internal surface area and pore volume, mesoporous nanoparticles are excellent devices for the storage and release of bioactive molecules such as antibacterial reagents and antibiotics.[10–12] Recent research indicates that biomaterials containing calcium (Ca) and silicate (Si) elements promote osteogenic differentiation of stem cell in vitro and hard tissue regeneration in vivo.[13,14] In this regard, mesoporous Ca-Si nanoparticles (MCSNs) possess both the merits of mesoporosity and the capability to release Ca and silicic acid ions.

Correspondence: Bing Fan
The State Key Laboratory Breeding Base of Basic Science of Stomatology (Hubei-MOST) and Key Laboratory of Oral Biomedicine Ministry of Education, School and Hospital of Stomatology, Wuhan University, 237 Luoyu Road, Wuhan 430079, People's Republic of China
Tel +86 27 8768 6210
Fax +86 27 8787 3260
Email bingfan8@hotmail.com

To be effective in infection control, antibacterial reagents are required to be incorporated into biomaterials either physically or chemically. Broad-spectrum antibiotics such as ampicillin are often used for such a purpose because they produce rapid and definitive antibacterial effects.[15] However, systemic toxicity has been reported in patients wearing antibiotic-loaded orthopedic prostheses.[16] The frequent use of antibiotic-loaded biomaterials may also increase the possibility of antibiotic resistance.[17,18] Inorganic metal such as silver (Ag) or metal ions such as silver ion (Ag^+) or zinc ion are alternatives to antibiotics because they possess broad spectrum bactericidal effects and show no evidence of tolerance and resistance by target bacteria.[19,20] Thus, many researchers have incorporated antibacterial metal or metal ions into biomaterials, such as mesoporous bioglass or silica nanoparticles, to achieve both antibacterial and pro-osteogenic effects.[12,21,22]

Two strategies have been employed for incorporating antibacterial metal or metal ions into biomaterials: adsorption and templating.[12,20,22,23] For mesoporous biomaterials, the adsorption method was most often used for loading antibacterial reagents because of its simplicity.[10,23] However, the loading amount of antibacterial metal or metal ions can be more easily controlled by the template method, and the metal or metal ions loaded by the template method are more stable in the carrier material.[11] To date, it is not known whether mesoporous materials loaded with antibacterial metal or metal ions by the template method exhibit similar antibacterial effects to those materials loaded by the adsorbed method. Thus, the objective of the present study was to evaluate the antibacterial effects of adsorbed and templated nanosilver in MCSNs. Specifically, the ability of these two versions of MCSNs in inhibiting the colonization of *Enterococcus faecalis* through adhesion and infiltration of dentin surfaces was examined. The null hypothesis tested was that there is no difference in the ability of adsorbed or templated nanosilver in MCSNs to inhibit the colonization of *E. faecalis* on intraradicular dentin.

Materials and methods

Synthesis and characterization of MCSNs and nanosilver incorporated MCSNs

All chemicals were obtained from Sigma-Aldrich (St Louis, MO, USA) unless otherwise stated and were used without further purification. MCSNs were synthesized according to our previously described method.[13] Briefly, 6.6 g of cetyltrimethylammonium bromide (CTAB) and 12 mL of ammonium hydroxide were dissolved in 600 mL of deionized water with stirring for 30 minutes. Then, 30 mL of tetraethyl orthosilicate (TEOS) and 31.21 g of calcium nitrate tetrahydrate were added with vigorous stirring for 3 hours. The products were collected by filtration and washed three times each with deionized water and ethanol. Then, the collected powders were dried at 60°C overnight and calcined at 550°C for 2 hours to remove remaining traces of CTAB.

For nanosilver incorporated MCSNs (Ag-MCSNs) prepared by the template method, the same procedures were employed, except that 3 g of silver nitrate ($AgNO_3$) (Reagent no 1; Factory of Shanghai Chemical Reagent Co., Ltd, Shanghai, People's Republic of China) were added together with 30 mL of TEOS and 31.21 g of calcium nitrate tetrahydrate. The obtained powders were designated as Ag-MCSNs-T.

For Ag-MCSNs prepared by the adsorption method, 20 mg of MCSNs was mixed with 10 mL of 1% $AgNO_3$ solution and stirred for 24 hours at room temperature. The mixture was centrifuged at 10,000 rpm for 10 minutes, and the supernatant was collected. The obtained powders were dried at 60°C overnight and designated as Ag-MCSNs-A. The loading efficiency of Ag was determined using inductively coupled plasma-atomic emission spectrometry (ICP-AES) (IRIS Intrepid II XSP; Thermo Fisher Scientific, Waltham, MA, USA) by calculating the ratio between the amount of absorbed Ag and the weight of MCSNs.

The prepared MCSNs and Ag-MSCNs were characterized by field emission-scanning electron microscopy (FE-SEM) (Ultraplus; Zeiss, Oberkochen, Germany), transmission electron microscopy (TEM) (JEM-2100; JEOL, Tokyo, Japan), and energy dispersive spectrometry (EDS) (X-Max50; Oxford Instruments, Abingdon, UK). The Brunauer–Emmett–Teller and the Barrett–Joyner–Halenda analyses were used to examine the specific surface area, pore volume, and pore size distribution by nitrogen adsorption–desorption isotherms (ASAP 2020; Micromeritics, Norcross, GA, USA).

Ion release and pH measurement of MCSNs and Ag-MCSNs

Twenty milligrams of MCSNs, Ag-MCSNs-A, or Ag-MCSNs-T was soaked in 10 mL of Tris-HCl (1 M, pH 7.4) at 37°C for 1, 3, 6, and 9 days. At each time point, a 5 mL aliquot of the solution was retrieved for measuring the released Ca ion (Ca^{2+}), Si ion (SiO_3^{2-}), and Ag^+ concentration by ICP-AES. The retrieved solution was replaced with 5 mL of fresh Tris-HCl. Testing was performed in triplicate for each group. The total amount of ions released at each time point from the Ag-MCSNs and MCSNs was calculated. For pH measurement of MCSNs and Ag-MCSNs, 150 mg

of MCSNs, Ag-MCSNs-A, or Ag-MCSNs-T was soaked in 30 mL double-distilled water at 37°C. The pH change over time was measured using a pH meter (Sartorius AG, Goettingen, Germany) at 1, 3, 6, and 9 days. Measurement was also performed in triplicate for each material.

Antibacterial effect of Ag-MCSNs

The antibacterial effects of the different nanoparticles were tested on *E. faecalis* (ATCC 29212; American Type Culture Collection (ATCC), Manassas, VA, USA). A 1 mL suspension (1×10^4 colony-forming units [CFUs]/mL) of *E. faecalis* and 5 mg of MCSNs, Ag-MCSNs-A, or Ag-MCSNs-T were mixed and incubated at 4°C for 24 hours. Then, 10 µL of the inoculums was plated on brain heart infusion broth agar (Becton Dickinson, Franklin Lakes, NJ, USA) and incubated at 37°C for 24 hours. Bacteria inoculum without nanoparticles was used as the negative control. The test was performed six times for each group, and CFUs of *E. faecalis* were counted for group comparisons.

Adhesion and infiltration test on dentin

Human single-rooted mandibular premolars with mature apices were collected under a protocol approved by the Ethics Committee of the School and Hospital of Stomatology, Wuhan University. The crowns of the teeth were removed, and the root lengths were standardized to 12 mm long. Working length was established at 1 mm short of the anatomical apex. Pulpal tissues were removed from each root canal, and the latter was instrumented with ProTaper nickel titanium rotary instruments (Dentsply Tulsa Dental Specialties, Tulsa, OK, USA) to size F3. A 6 mL volume of 5.25% sodium hypochlorite was used as the initial irrigant, and 6 mL of 17% ethylenediaminetetraacetic acid was used as final irrigant to completely remove dentinal debris on the canal wall that was produced during the canal enlarging process. The instrumented canals were finally rinsed with copious tap water and dried with paper points. The roots were then split into two halves longitudinally in the buccolingual direction with a hammer and chisel to expose the canal wall dentin surface, with patent dentin tubule openings and the split dentin surface with axial cross-sections of tubules (Figure 1G). The cleanliness of the root canal walls was confirmed using FE-SEM.

To observe the adhesion of Ag-MCSNs on canal wall dentin and their infiltration into dentinal tubules, 20 mg/mL of Ag-MCSNs-A suspension was prepared in sterile distilled water and injected into the canals (Figure 1A). Conventional calcium hydroxide ($Ca[OH]_2$) powder (particle size in microscale confirmed by FE-SEM [data not shown]) (Sigma-Aldrich) was used as the control. The suspension in the root canals was subjected to passive ultrasonic vibration by inserting an ultrasonic needle into the canal to a depth of 11 mm. The power of the ultrasonic device (P5; Satelec, Merignac, France) was set at scale 4, which is suitable for ultrasonic canal irrigation in clinical treatment. Ultrasonic vibration lasted for 60 seconds (Figure 1B). The canals were subsequently dried with sterile paper points and rinsed with 5 mL of sterile distilled water (Figure 1C). After further drying with sterile paper points, the roots were stored at 60°C for 12 hours.

The roots were then split into two halves as described above (Figure 1E). FE-SEM was used to observe the adhesion of Ag-MCSNs-A on the dentin surface and the infiltration of nanoparticles into the dentinal tubules. Mapping of the elemental distribution was performed on the canal wall dentin to confirm the adhesion of Ag-MCSNs-A on dentin surfaces and the distribution of Ag, Ca, and Si elements (Figure 1E); EDS point analyses were performed on the particles inside the dentinal tubules to confirm the infiltration of Ag-MCSNs-A.

Bacterial colonization on root canal walls treated with different materials

Thirty roots were prepared as described previously and autoclaved for 20 minutes at 121°C in deionized water. The roots were divided randomly into five groups (N=6). Each instrumented canal was filled with 20 mg/mL suspension of MCSNs, Ag-MCSNs-A, Ag-MCSNs-T, or $Ca(OH)_2$ and activated by the ultrasonic device (Figure 1A–C). Root canals filled with deionized water were used as the control. The canals in each group were then thoroughly rinsed with 5 mL of sterile distilled water and dried with sterile paper point.

Each root canal was then filled with *E. faecalis* suspension (1×10^8 CFUs/mL) and incubated under anaerobic conditions at 37°C for 7 days (Figure 1D). At the end of the incubation period, the roots from each group were split into two halves as described (Figure 1F). One root-half was randomly selected from each root, which was stained with fluorescent LIVE/DEAD BacLight bacterial viability stain (Molecular Probes, Eugene, OR, USA) according to the manufacturer's instructions. The stained root-halves were examined using confocal laser scanning microscopy (CLSM) (Nikon A1 Si; Nikon Corporation, Tokyo, Japan). The excitation/emission wavelengths were 500/530 nm for SYTO 9 and 552/617 nm for propidium iodide, respectively. Three randomly selected canal wall dentin areas from the coronal, middle, and apical third (Figure 1G) of each root were scanned by CLSM with a

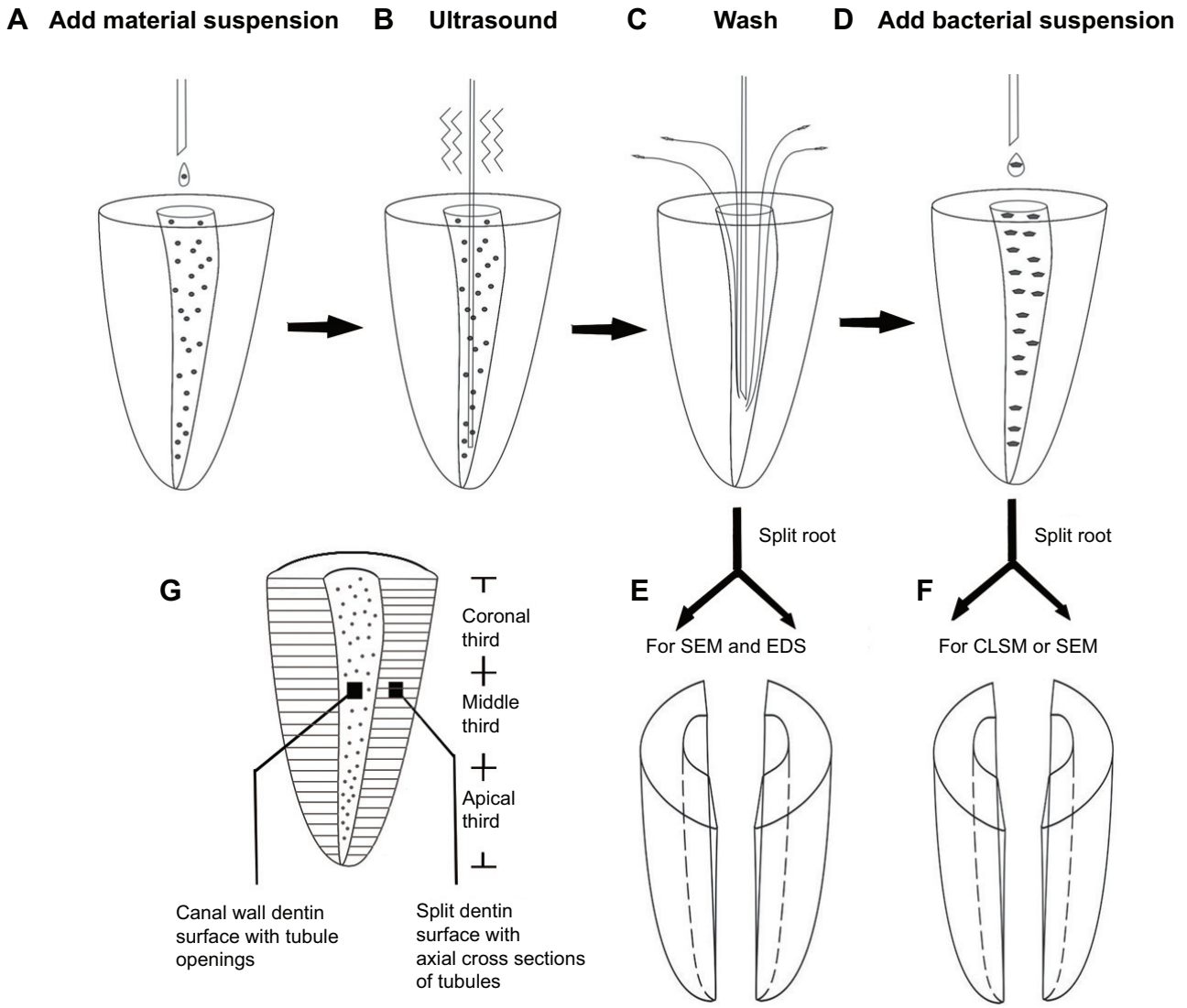

Figure 1 Schematic illustration of the experimental procedures performed on extracted teeth.
Notes: (**A**) Material suspension was injected into the root canals; (**B**) material suspensions were subjected to passive ultrasonic activation; (**C**) canals were washed with sterile distilled water; (**E**) the roots were split into two halves to observe the adhesion and infiltration of materials on dentin surfaces; (**D**) *Enterococcus faecalis* suspension was added into the canals and incubated for 1 week; (**F**) the roots were split into two halves to observe *E. faecalis* adherence and colonization on dentin surfaces; (**G**) different dentin surfaces for observations.
Abbreviations: CLSM, confocal laser scanning microscopy; EDS, energy dispersive spectrometry; SEM, scanning electron microscopy.

Z-step size of 2 μm. Simultaneous dual-channel imaging was used to display green fluorescence (live cells) and red fluorescence (dead cells). Biovolumes representing the amount of bacteria were calculated from the total fluorescence and averaged among the selected areas of each root sample using the software NIS-Elements AR (Nikon Corporation). To test the background fluorescence produced by nanoparticles, one root treated with only MCSNs suspension but without bacteria seeding was also observed using CLSM.

To identify the morphology and distribution of bacteria and materials on dentin, one randomly selected root-half from each group was observed using FE-SEM. Briefly, the specimens were immersed in 4% glutaraldehyde in 0.1 mol/L sodium cacodylate buffer, dehydrated through ascending grades of ethanol, dried with a critical point dryer, and sputter-coated with gold in a vacuum evaporator (Hitachi E-1045; Hitachi Ltd., Tokyo, Japan).

Cytotoxicity test

To test the cytotoxicity of different materials, the cell counting kit-8 (CCK-8) (Dojindo Laboratories, Kumamoto, Japan) method was performed on human bone marrow mesenchymal cells (BMSCs) (ATCC) according to manufacturer's instructions. Briefly, 3×10^3 cells suspended in 100 μL low glucose Dulbecco's Modified Eagle's Medium (DMEM) (Thermo Scientific) supplemented with 10% fetal calf serum

(FCS) (Thermo Scientific) and 1% penicillin/streptomycin (Thermo Scientific) were seeded into each well of a 96-well plate. After 48 hours incubation at 37°C, 5% CO_2 for cell attachment, 10 µL of different material extracts with different concentrations (prepared by soaking 10, 20, and 40 mg materials in 1 mL double-distilled water at 37°C for 24 hours) was added into different wells. The wells containing only DMEM and the wells containing cells without extracts were used as controls. Each group described above had six wells. After 48 hours of incubation, the media in each well were removed and washed three times with DMEM, and 100 µL fresh phenol-red-free culture media was added into each well. A volume of 10 µL of CCK-8 solution was then added into each well and incubated for 4 hours. The absorbance was measured at 450 nm using a microplate reader (Power Wave XS2; BioTek Instruments, VT, USA).

Statistical analysis

Because the normality and equal variance assumptions of the data were violated, the data were analyzed using Kruskal–Wallis analysis of variance. Post hoc pairwise comparisons were performed using the Mann–Whitney *U*-test. Statistical significance was preset at P=0.05.

Results

Characterizations of MCSNs and Ag-MCSNs

SEM images showed that MCSNs and Ag-MCSNs nanoparticles were irregular in shape, with a diameter of approximately 200 nm (Figure 2A–C). TEM showed that MCSNs and Ag-MCSNs-T had well-ordered nanopores and channel structures (Figure 2D, F, G, and I). These ultrastructural features were obscured in the Ag-MCSNs-A, and numerous black dots were trapped within the nanoparticles (Figure 2E and H). Black dots were also present and were evenly distributed within the Ag-MCSNs-T nanoparticles (Figure 2F and I). The ion release experiment performed by ICP-AES indicated that the Ag loading efficiency of Ag-MCSNs-A was 25.2%±1.9%. The EDS analysis spectrum confirmed the presence of Ca and Si elements in MCSNs and Ag-MCSNs, and Ag in Ag-MCSNs (Figure 3A, D, and G). The proportion of each element is shown in Table 1. Nitrogen adsorption–desorption

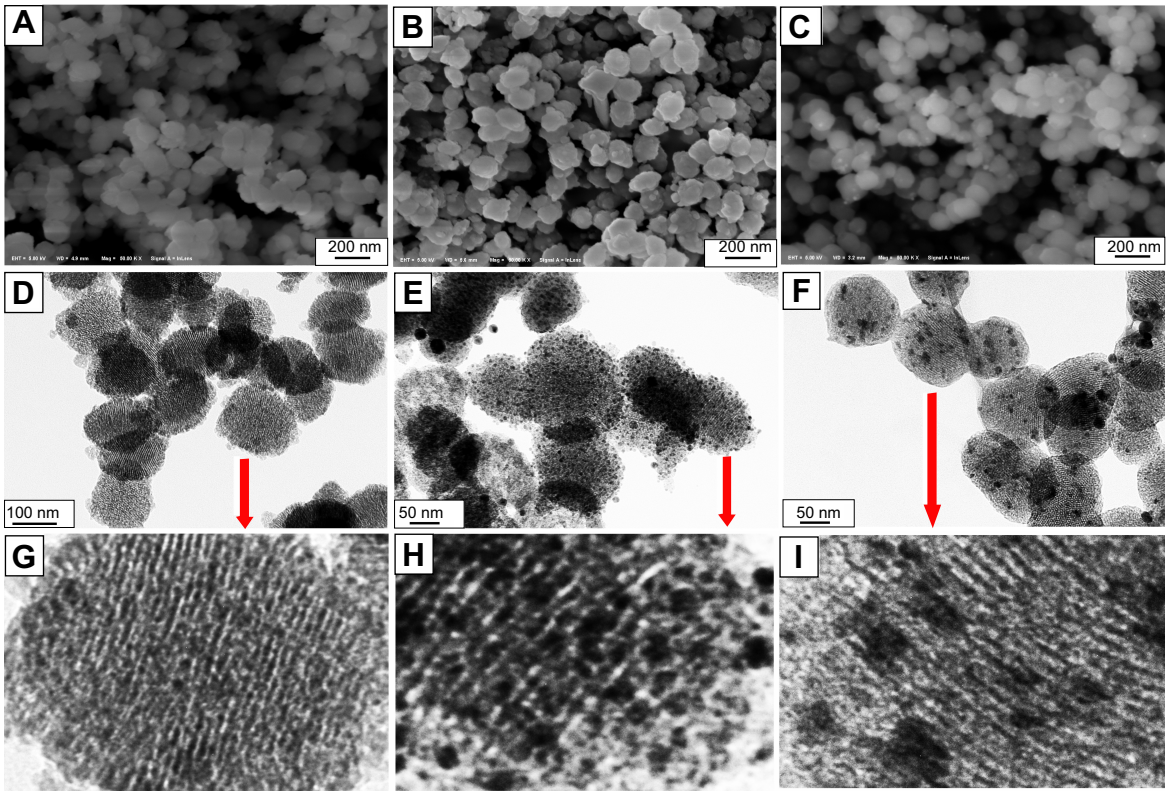

Figure 2 SEM and TEM images of nanoparticles.
Notes: SEM images of MCSNs, Ag-MCSNs-A, and Ag-MCSNs-T particles (**A**, **B**, and **C**, respectively); TEM images of MCSNs, Ag-MCSNs-A and Ag-MCSNs-T particles (**D**, **E**, and **F**, respectively); zoom-in images from the selected area (arrows) in D, E, and F (**G**, **H**, and **I**, respectively).
Abbreviations: Ag-MCSNs-A, nanosilver-incorporated MCSNs prepared by the adsorption method; Ag-MCSNs-T, nanosilver-incorporated MCSNs prepared by the template method; MCSNs, mesoporous calcium-silicate nanoparticles; SEM, scanning electron microscopy; TEM, transmission electron microscopy.

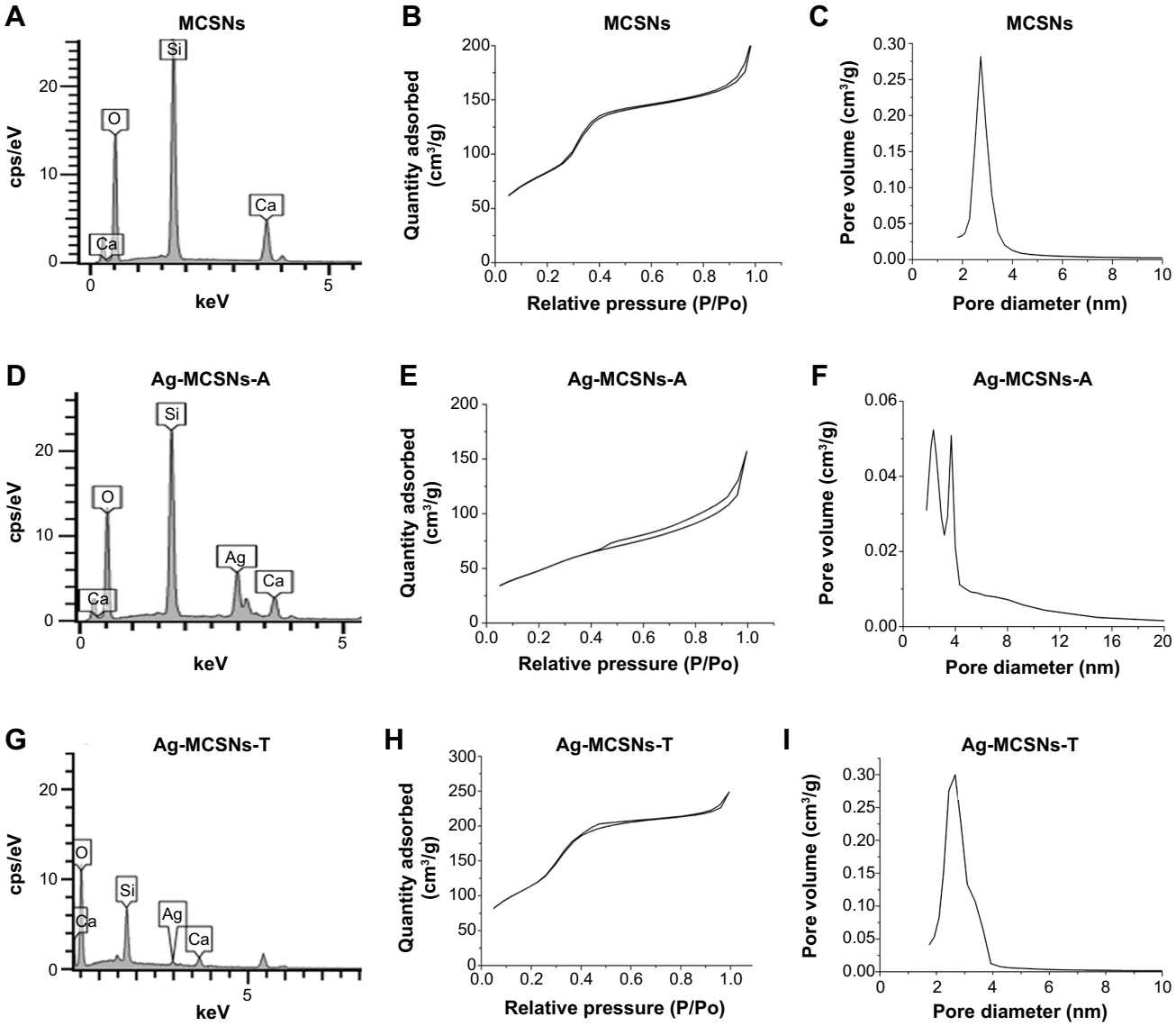

Figure 3 Characterization of nanoparticles.

Notes: EDS results of MCSNs, Ag-MCSNs-A, and Ag-MCSNs-T particles (**A**, **D**, and **G**, respectively); nitrogen adsorption–desorption isotherm test of MCSNs, Ag-MCSNs-A, and Ag-MCSNs-T particles (**B**, **E**, and **H**, respectively); pore size distribution of the MCSNs, Ag-MCSNs-A, and Ag-MCSNs-T (**C**, **F**, and **I**, respectively).

Abbreviations: Ag-MCSNs-A, nanosilver-incorporated MCSNs prepared by the adsorption method; Ag-MCSNs-T, nanosilver-incorporated MCSNs prepared by the template method; EDS, energy dispersive spectrometry; MCSNs, mesoporous calcium-silicate nanoparticles.

isotherm of these nanoparticles revealed type IV isotherms with H1-type hysteresis loops (Figure 3B, E, and H). The pore diameter was mostly in the range of 2–4 nm (Figure 3C, F, and I). The surface area, pore volume, and mean pore size of MCSNs and Ag-MCSNs are presented in Table 2.

Ion release and pH change over time

All the nanoparticles were found to have a sustained release of ions over 9 days in Tris-HCl (Figure 4). The Ag-MCSNs-A released Ag^{+} faster than the Ag-MCSNs-T over time (indicated by the slope of curve in Figure 4). In addition, the Ca^{2+} and SiO_3^{2-} released from Ag-MCSNs-A were less than those released by Ag-MCSNs-T. The two versions of Ag-MCSNs released less Ca^{2+} and SiO_3^{2-} than MCSNs. The pH of MCSNs and Ag-MCSNs was found stable at about 9 over time (Figure 4). The addition of nanosilver by either adsorption or template method did not affect the pH of MCSNs significantly (Figure 4).

Antibacterial effect

The Ag-MCSNs-A and Ag-MCSNs-T showed better antibacterial properties than the MCSNs and the blank control ($P<0.05$) (Figure 5), with no significant difference between the two versions of silver-containing MCSNs. Interestingly, the

Table 1 Quantitative EDS analysis of the element proportion in the nanoparticles (weight %)

Nanoparticles	O	Si	Ca	Ag
MCSNs	61.84	28.68	9.47	–
Ag-MCSNs-A	49.76	23.82	5.09	21.33
Ag-MCSNs-T	48.13	34.21	10.02	7.63

Abbreviations: Ag-MCSNs-A, nanosilver-incorporated MCSNs prepared by the adsorption method; Ag-MCSNs-T, nanosilver-incorporated MCSNs prepared by the template method; EDS, energy dispersive spectrometry; MCSNs, mesoporous calcium-silicate nanoparticles.

nonsilver-containing MCSNs exhibited relatively better antibacterial effect than the blank control ($P<0.05$) (Figure 5).

Dentinal tubule infiltration

Images acquired by FE-SEM showed dentinal tubule orifices on the canal wall were clean after root canal instrumentation (Figure 6A) or after treatment with $Ca(OH)_2$ suspension (Figure 6B). After passive ultrasonic treatment with Ag-MCSNs-A suspension, the canal wall and dentinal tubule orifices were covered with nanoparticles, even after canal rinsing (Figure 6C). Numerous nanoparticles aggregated around the tubular orifice and infiltrated the dentinal tubules (Figure 6D). The presence of these nanoparticles was confirmed by EDS-mapping analysis (Figure 6E–G).

Examination of the split longitudinal sections of the dentinal tubules revealed that $Ca(OH)_2$ particles did not enter the dentinal tubules (Figure 6H). By contrast, Ag-MCSNs-A nanoparticles infiltrated the dentinal tubules to a maximum depth of 20 μm (Figure 6I and J); EDS point analysis confirmed the infiltration of Ag-MCSNs-A nanoparticles into dentinal tubules (Figure 6K).

Bacterial adherence and colonization on root canal wall

Three dimensional reconstructions of CLSM images showed very weak background fluorescence produced by MCSNs that adhered to the canal wall (Figure 7B). For the blank control, $Ca(OH)_2$ and MCSNs groups, strong green fluorescence from live *E. faecalis* was observed on the root canal walls (Figure 7C–E). The Ag-MCSNs-A and Ag-MCSNs-T groups showed much weaker fluorescence, indicating that bacteria adhered and colonized only sparsely on the canal walls (Figure 7F and G). Red fluorescence was very weak and scarcely observed in each group.

The total fluorescence from the bacteria was calculated as the biovolume (μm^3 per field of view) to quantify the amount of bacteria. There were no significant differences among the mean biovolume of the blank control, $Ca(OH)_2$ and MCSNs groups ($P>0.05$) (Figure 7A). The mean biovolumes of these groups were significantly higher than those derived from the Ag-MCSNs-A and Ag-MCSNs-T groups ($P<0.05$). The mean biovolume in the Ag-MCSNs-A group was significantly less than the Ag-MCSNs-T group ($P<0.05$).

SEM images of split-fractured root-halves showed that numerous *E. faecalis* cells colonized on the root canal wall and started to grow into dentinal tubules in blank control, $Ca(OH)_2$ and MCSNs groups (Figure 8A–C). The lowest amount of bacteria colonization was observed in Ag-MCSNs-A and Ag-MCSNs-T groups (Figure 8D and G). Some bacteria that were in direct contact with Ag-MCSNs exhibited perforated or deformed cell membranes; these features were suggestive of cell death associated with those bacteria cells (Figure 8E, F, H, and I).

Table 2 Surface area (S_{BET}), pore volume (V_P), and mean pore size (D_P) of the nanoparticles

Materials	S_{BET} ($m^2\ g^{-1}$)	V_P ($cm^3\ g^{-1}$)	D_P (nm)
MCSNs	308.89	0.33	4.24
Ag-MCSNs-A	180.35	0.24	5.39
Ag-MCSNs-T	449.46	0.38	3.42

Abbreviations: Ag-MCSNs-A, nanosilver-incorporated MCSNs prepared by the adsorption method; Ag-MCSNs-T, nanosilver-incorporated MCSNs prepared by the template method; MCSNs, mesoporous calcium-silicate nanoparticles.

Cytotoxicity of materials

The CCK-8 test revealed that Ag-MCSNs with adsorbed nanosilver showed significantly higher cytotoxicity on BMSCs when compared with MCSNs or Ag-MCSNs with templated nanosilver ($P<0.05$) (Figure 9). Both MCSNs and Ag-MCSNs-T showed no obvious cytotoxicity on BMSCs as no significant difference was found between the blank control and the MCSNs or Ag-MCSNs-T groups ($P>0.05$) (Figure 9). There was also no significant difference in cytotoxicity among different extract concentrations for either MCSNs or Ag-MCSNs-T groups ($P>0.05$) (Figure 9).

Discussion

In the present study, nanosilver (appearing as electron-dense dots under TEM) was successfully incorporated into MCSNs through adsorption and template methods. The mechanism for the formation of MCSNs with templated nanosilver (Ag-MCSNs-T) has not yet been studied in depth but could be similar to that of MCSNs: the CTAB provided a template for interactions and combination between the Si (TEOS) and the metal elements, ie, Ca (from $Ca[NO_3]_2$) and Ag (from $AgNO_3$) to form the skeleton of mesoporous structures. The Ag-MCSNs-T nanoparticles presented a typical

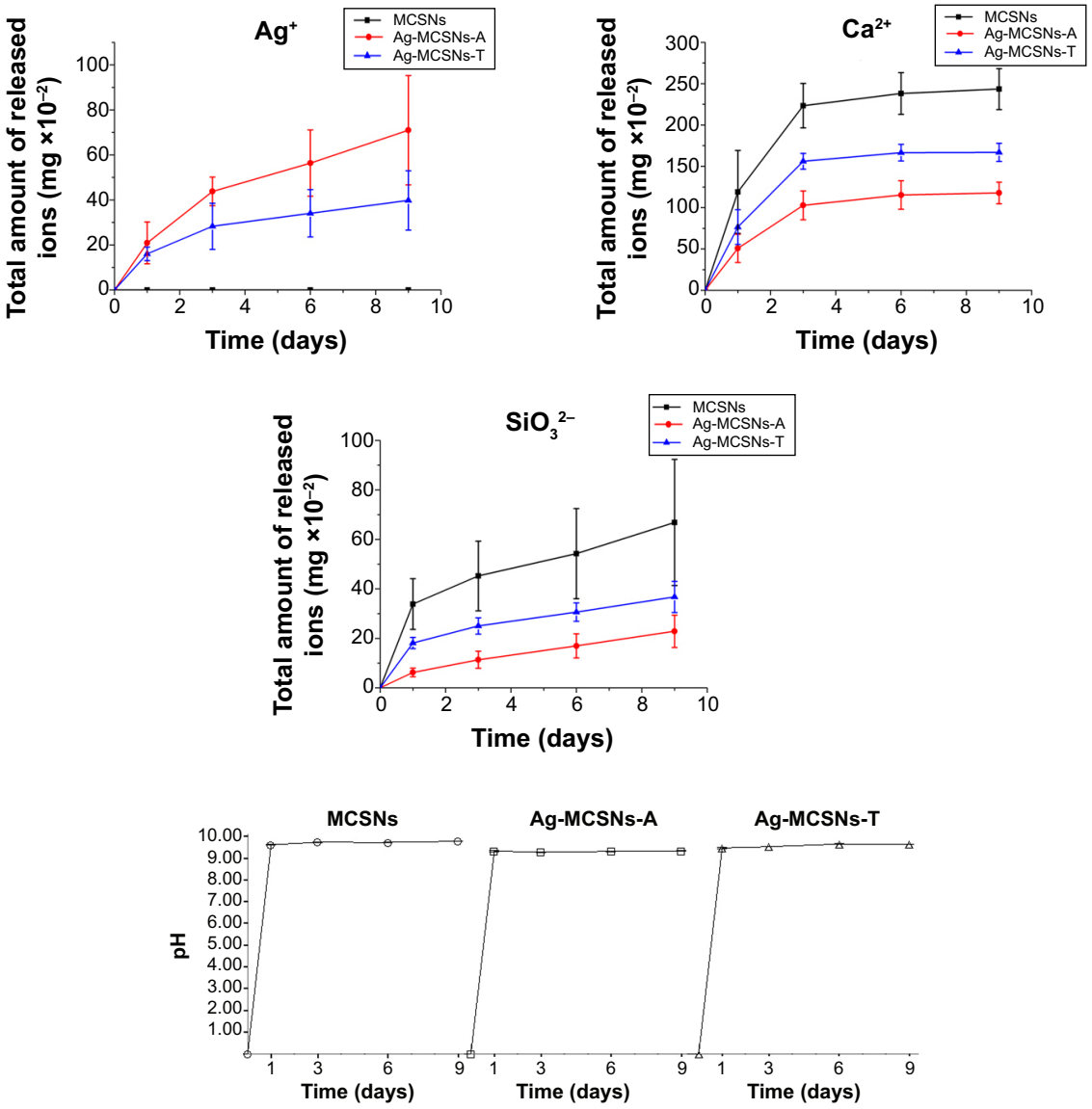

Figure 4 Ag^+, Ca^{2+}, and SiO_3^{2-} ion release profile and pH measurement of MCSNs, Ag-MCSNs-A, and Ag-MCSNs-T over time.
Abbreviations: Ag-MCSNs-A, nanosilver-incorporated MCSNs prepared by the adsorption method; Ag-MCSNs-T, nanosilver-incorporated MCSNs prepared by the template method; MCSNs, mesoporous calcium-silicate nanoparticles.

mesoporous structure as the MCSNs, and the nanosilver was distributed evenly inside the mesoporous structure. The ion-releasing profiles of Ag-MCSNs-T approximated those of Ag-MCSNs-A. All these findings indicated that antibacterial nanosilver incorporated into mesoporous nanoparticles through the template method could be released in a sustained manner in the form of Ag^+.[24,25] Mesoporous nanoparticles with templated nanosilver may be further used for storing other bioactive molecules in their mesoporous structures to produce multifunctional biomaterials.

Although both Ag-MCSNs-A and Ag-MCSNs-T demonstrated sustained release of Ag^+ over a 9-day period, Ag-MCSNs-T had a slower release rate than Ag-MCSNs-A. Sustained release of an antimicrobial agent is important for root canal disinfection, and the antibacterial effects of Ag-MCSNs-A or Ag-MCSNs-T can be maintained for a relatively long time. It is anticipated that the antibacterial effect of MCSNs with templated nanosilver will last longer than the MCSNs carrying adsorbed nanosilver. Both Ca^{2+} and SiO_3^{2-} were also found to be released in a sustained manner by both Ag-MCSNs nanoparticles, thereby contributing to biomineralization and hard tissue regeneration.[13] Despite this, the Ag-MCSNs-A showed a severe cytotoxicity as compared to Ag-MCSNs-T, which could also be due to its greater and more rapid release of Ag^+. Based on these results, the Ag-MCSNs-T could be a more desirable candidate for intracanal

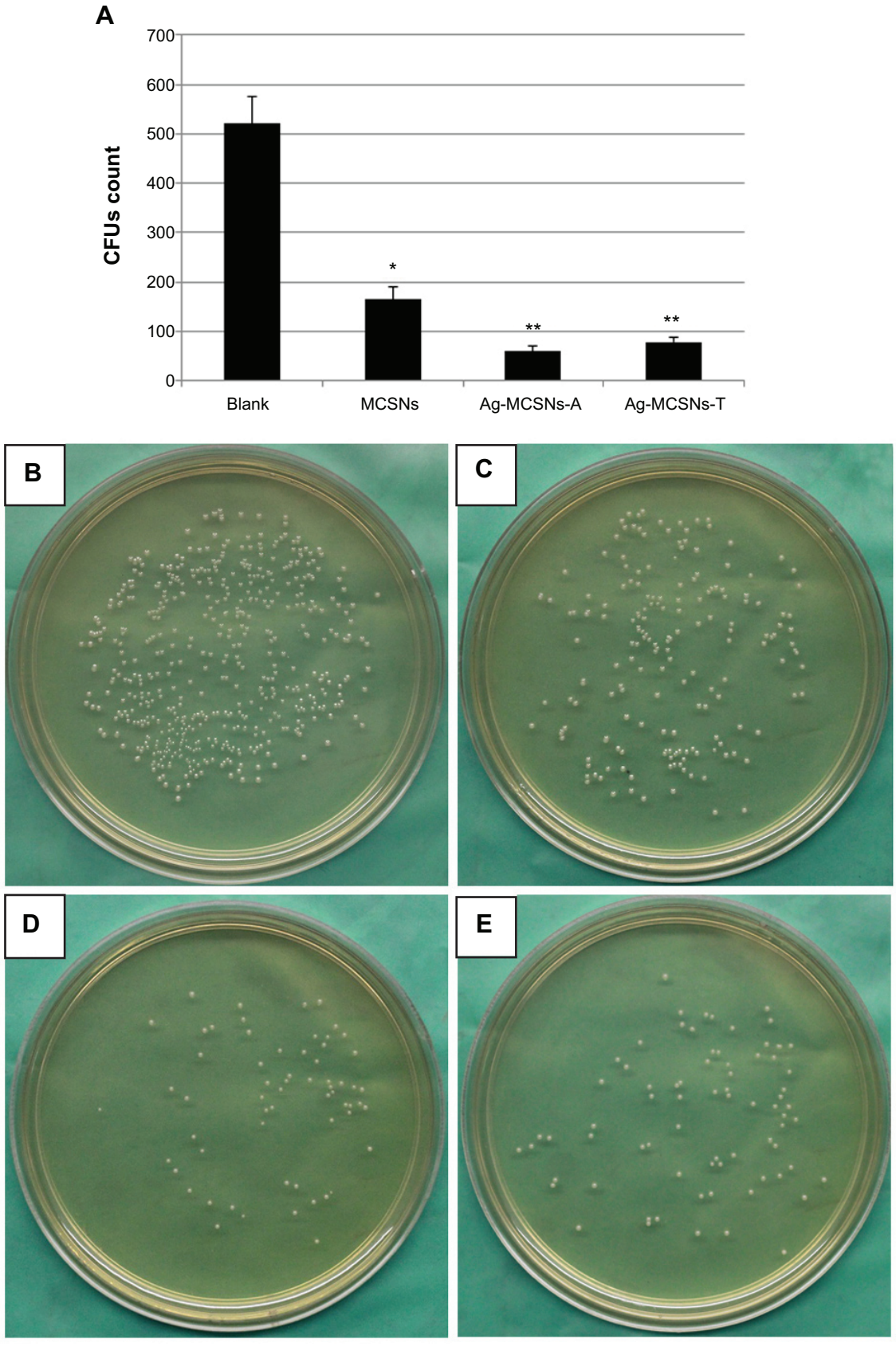

Figure 5 Antibacterial effect of MCSNs, Ag-MCSNs-A, and Ag-MCSNs-T.
Notes: (**A**) CFUs count among different groups (columns designated with different asterisk numbers are significantly different from each other [$P<0.05$]); (**B**–**E**) bacteria colonies cultured on agar plates in the blank control (**B**), MCSNs (**C**), Ag-MCSNs-A (**D**), and Ag-MCSNs-T (**E**) groups.
Abbreviations: Ag-MCSNs-A, nanosilver-incorporated MCSNs prepared by the adsorption method; Ag-MCSNs-T, nanosilver-incorporated MCSNs prepared by the template method; CFUs, colony-forming units; MCSNs, mesoporous calcium-silicate nanoparticles.

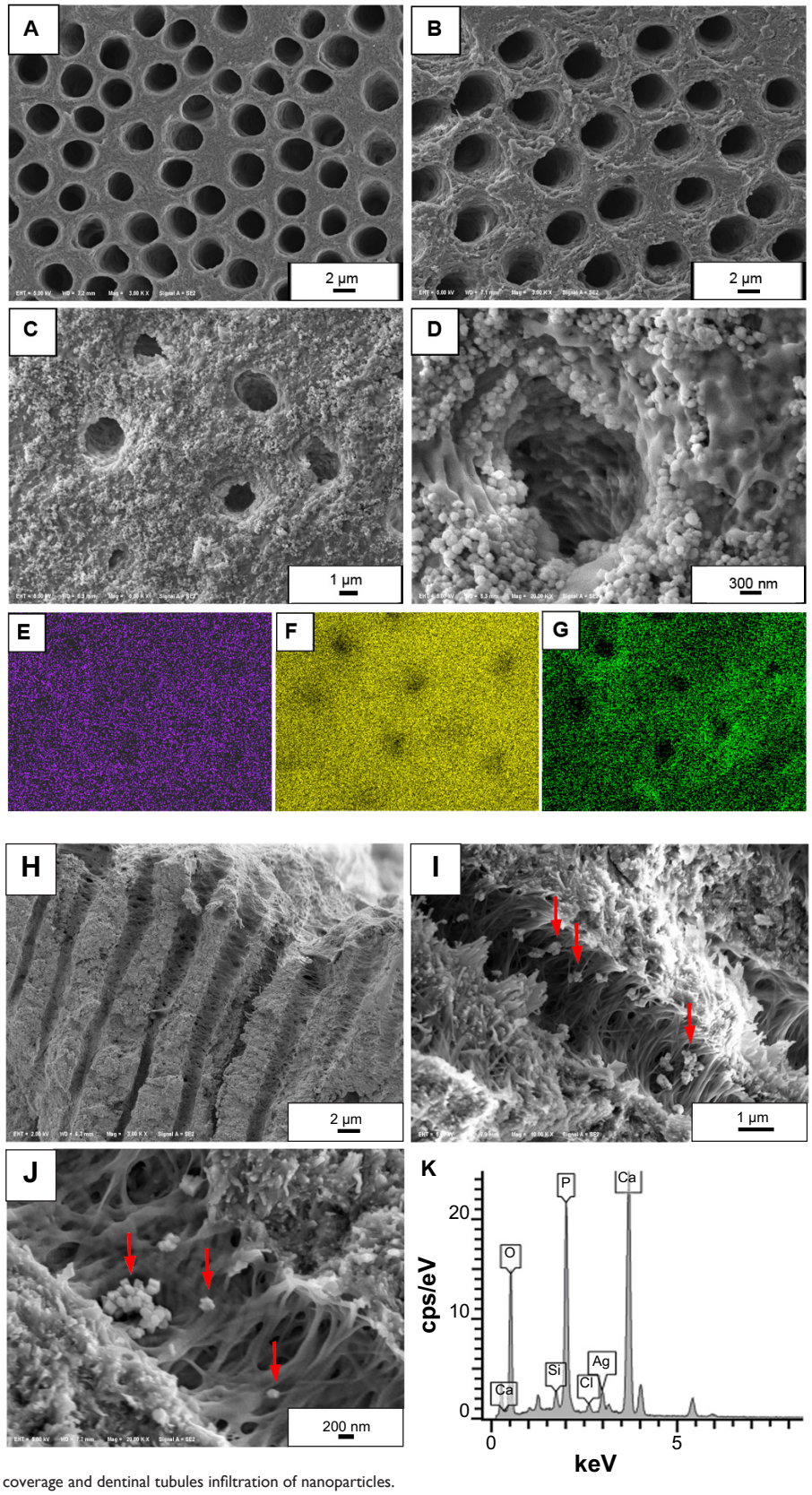

Figure 6 Root canal wall coverage and dentinal tubules infiltration of nanoparticles.

Notes: (**A**) Dentinal tubule orifices after root canal enlargement; (**B**) dentinal tubule orifices after treatment with $Ca(OH)_2$; (**C** and **D**) nanoparticles covering the root canal wall and aggregating around the dentinal tubule orifices, with some nanoparticles infiltrating the tubules; (**E**, **F**, and **G**) elemental mappings show the presence of Ag, Ca, and Si in the nanoparticles covering the root canal wall; (**H**) $Ca(OH)_2$ did not enter the dentinal tubules; (**I** and **J**) nanoparticles infiltrated the dentinal tubules (arrows); (**K**) EDS confirmed the presence of Ag, Ca, and Si in the nanoparticles within the dentinal tubules.

Abbreviations: EDS, energy dispersive spectrometry.

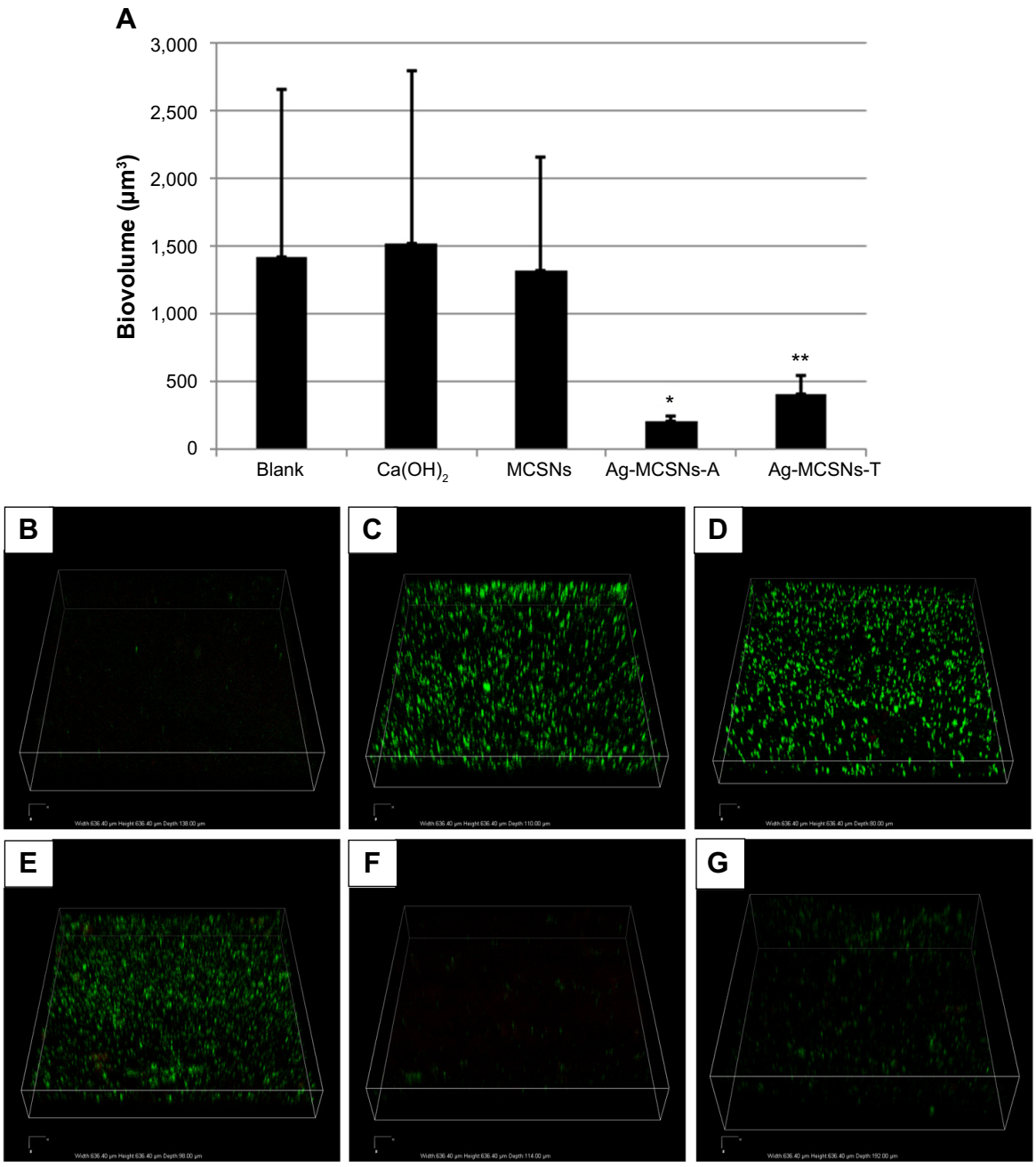

Figure 7 *Enterococcus faecalis* adherence and colonization on the root canal wall as observed by CLSM.
Notes: (**A**) Comparison of biovolumes calculated from the total fluorescence among groups (columns designated with different asterisk numbers are significantly different [$P<0.05$]); (**B**) background fluorescence produced by MCSNs; representative reconstructed CLSM images of the (**C**) blank control group; (**D**) $Ca(OH)_2$ (calcium hydroxide) group; (**E**) MCSNs group; (**F**) Ag-MCSNs-A group; and (**G**) Ag-MCSNs-T group.
Abbreviations: Ag-MCSNs-A, nanosilver-incorporated MCSNs prepared by the adsorption method; Ag-MCSNs-T, nanosilver-incorporated MCSNs prepared by the template method; CLSM, confocal laser scanning microscopy; MCSNs, mesoporous calcium-silicate nanoparticles.

disinfectant as it possessed both a sustained release of Ag^+ and low cytotoxicity.

In the planktonic antibacterial test, both Ag-MCSNs nanoparticles groups showed significant higher antibacterial effects than the MCSNs groups, indicating that the antibacterial mechanism of Ag-MCSNs is related to the released Ag^+ rather than the Ca^{2+} or SiO_3^{2-}. The MCSNs also demonstrated mild antibacterial effects when compared with the blank control. This is in agreement with our previous study,[13] although the mechanism responsible for the antibacterial activity of MCSNs against planktonic *E. faecalis* is not clear. A possible explanation is that the released Ca^{2+} and SiO_3^{2-} produce an alkaline microenvironment.[13] In addition, the nanodimension of MCSNs may interfere with bacteria

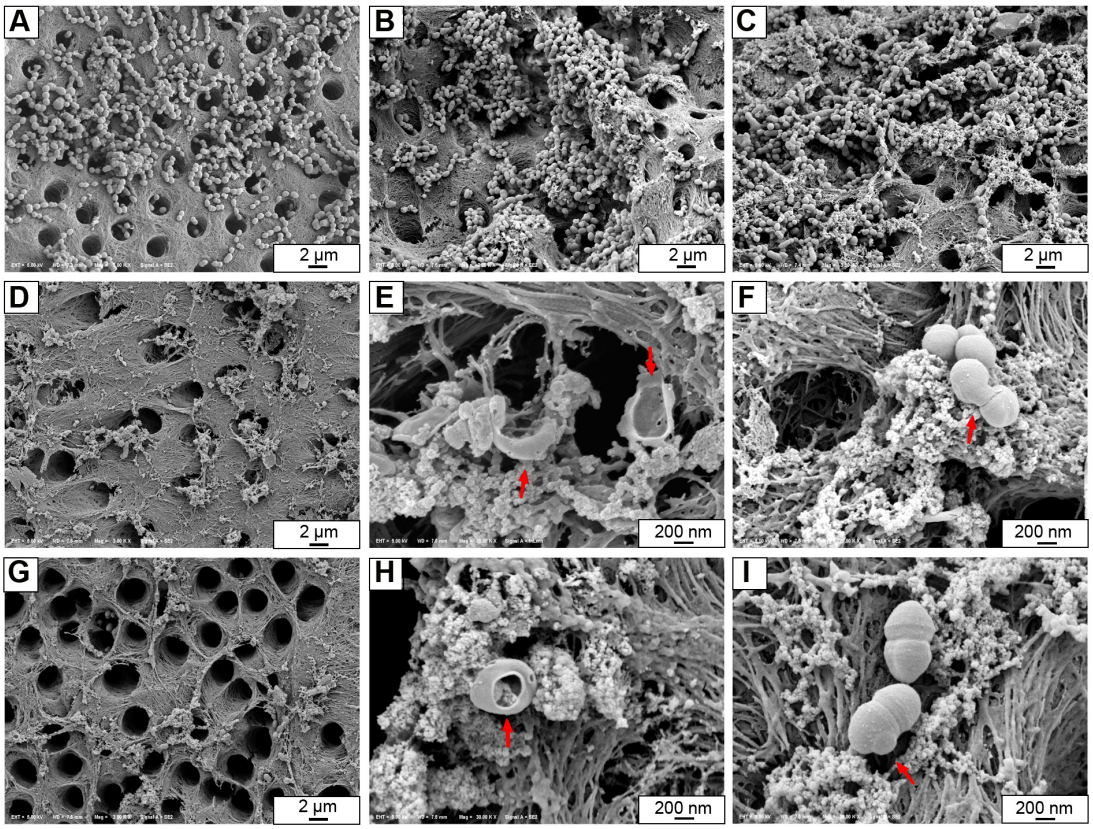

Figure 8 Representative FE-SEM images showing colonization of *Enterococcus faecalis* on root canal walls.
Notes: (**A**) Blank control group; (**B**) calcium hydroxide group; (**C**) MCSNs group; (**D**) Ag-MCSNs-A group; (**G**) Ag-MCSNs-T group; (**E** and **H**) dead bacteria in direct contact with Ag-MCSNs contained perforated membranes (arrows); (**F** and **I**) a bacterium in direct contact with Ag-MCSNs showing deformed cell membrane (arrows).
Abbreviations: Ag-MCSNs-A, nanosilver-incorporated MCSNs prepared by the adsorption method; Ag-MCSNs-T, nanosilver-incorporated MCSNs prepared by the template method; FE-SEM, field emission-scanning electron microscopy; MCSNs, mesoporous calcium-silicate nanoparticles.

metabolism,[26] especially when the nanoparticles are in direct contact with bacteria in a liquid environment. It is possible, however, that the antibacterial effect of MCSNs may be compromised in root canal systems containing bacteria biofilms instead of planktonic bacteria due to changes in interaction between the nanoparticles and bacteria.

Infection of dentinal tubules within the intraradicular dentin has been reported to occur in 70%–80% of the teeth with infection around the root apex.[27,28] Bacterial invasion into dentinal tubules has been shown to be one of the major causes of posttreatment reinfection.[29] Conventional intracanal disinfectants, such as $Ca(OH)_2$, showed compromised antibacterial effects and no substantivity against *E. faecalis*, especially after the medicament was removed before the root canal is obturated. This may be caused by the following: 1) The major antibacterial mechanism of $Ca(OH)_2$ is its high pH resulting from OH^- released; however, many species of infectious bacteria found in root canals, including *E. faecalis*, had developed resistance against the high pH of $Ca(OH)_2$;[30] 2) Conventional $Ca(OH)_2$ particles are

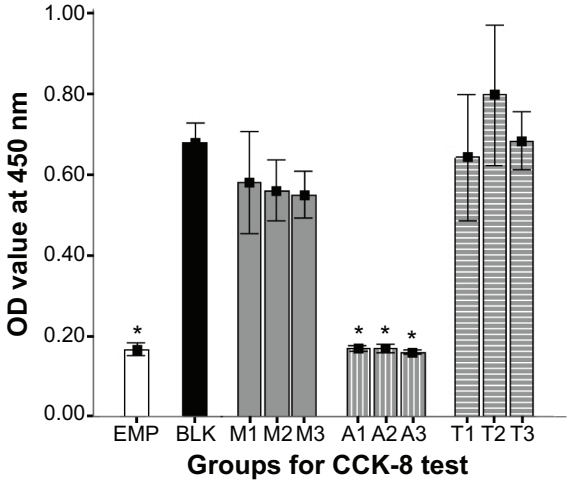

Figure 9 Cytotoxicity test on BMSCs.
Notes: EMP represents wells with only DMEM; BLK represents wells with cells but no added material extracts; M1–3: wells with 10 μL of 10, 20, and 40 mg/mL MCSNs extracts; A1–3: wells with 10 μL of 10, 20, and 40 mg/mL Ag-MCSNs-A extracts; T1–3: wells with 10 μL of 10, 20, and 40 mg/mL Ag-MCSNs-T extracts; *$P<0.05$.
Abbreviations: Ag-MCSNs-A, nanosilver-incorporated MCSNs prepared by the adsorption method; Ag-MCSNs-T, nanosilver-incorporated MCSNs prepared by the template method; BMSCs, bone marrow mesenchymal cells; CCK-8, cell counting kit-8; DMEM, Dulbecco's Modified Eagle's Medium; MCSNs, mesoporous calcium-silicate nanoparticles; OD, optical density.

normally supplied in the form of microparticles instead of nanoparticles (confirmed by SEM in our pilot experiment). This dimensional attribute seriously limits the ability of $Ca(OH)_2$ to adhere to and infiltrate dentin surfaces, rendering the microparticles easy to be rinsed off (Figure 6B and H). In the present study, the Ag-MCSNs nanoparticles adhere well to canal wall dentin and infiltrate the dentinal tubules after ultrasound activation, even after rinsing the root canals. These nanoparticles serve as a reservoir of Ag^+ to prevent and inhibit the bacteria recolonization and reinfection of the root canals. This feature was confirmed in the present study by CLSM examination. Green fluorescence, which is indicative of the presence of live bacteria, was significantly weaker in Ag-MCSNs groups. Red fluorescence, which is indicative of the presence of dead bacteria, was very weak in each group probably because the dead bacteria detached from the dentin surface much more easily than live bacteria during the specimen preparation procedures for CLSM. Admittedly, the Ag-MCSNs with templated nanosilver demonstrated weaker antibacterial activity on dentin surfaces when compared with Ag-MCSNs with adsorbed nanosilver. This phenomenon may be attributed to the relative slow release of Ag^+ during the 7-day period. Hence, the long-term antibacterial effects of Ag-MCSNs with templated nanosilver should be further investigated.

Based on the findings in this study, the MCSNs with templated nanosilver could be a more desirable biomaterial, with both greater antibacterial ability and lower cytotoxicity than the nanoparticles with conventionally-adsorbed nanosilver. These MCSNs with templated nanosilver could be further tested in infected bone defect areas to see if they can control bone infection and promote bone regeneration at the same time. They could also be used to carry other bioactive molecules, such as growth factors, to enhance their ability in tissue restoration.

Conclusion

Within the limits of the present study, it may be concluded that nanosilver can be successfully incorporated into MCSNs through a template method. The Ag-MCSNs-T exhibited similar antibacterial effects against *E. faecalis* in either planktonic or colonized form as the Ag-MCSNs-A but showed much lower cytotoxicity than Ag-MCSNs-A. The Ag-MCSNs-T may be developed into a new intracanal disinfectant for root canal disinfection due to its antibacterial ability and low cytotoxicity, and may be further used for infected bone defect restoration or to carry other bioactive molecules as a multifunctional biomaterial.

Acknowledgments

This study was financially supported by the National Natural Science Foundation of China (81271130), Natural Science Foundation of Hubei Province, China (2013CFB241) and the Innovation Seed Fund of School of Medicine, Wuhan University.

Disclosure

The authors report no conflicts of interest in this work.

References

1. Campoccia D, Montanaro L, Arciola CR. A review of the biomaterials technologies for infection-resistant surfaces. *Biomaterials.* 2013; 34(34):8533–8554.
2. Shi Z, Neoh KG, Kang ET, Wang W. Antibacterial and mechanical properties of bone cement impregnated with chitosan nanoparticles. *Biomaterials.* 2006;27(11):2440–2449.
3. Waltimo T, Mohn D, Paqué F, et al. Fine-tuning of bioactive glass for root canal disinfection. *J Dent Res.* 2009;88(3):235–238.
4. Nair PN, Henry S, Cano V, Vera J. Microbial status of apical root canal system of human mandibular first molars with primary apical periodontitis after "one-visit" endodontic treatment. *Oral Surg Oral Med Oral Pathol Oral Radiol Endod.* 2005;99(2):231–252.
5. Ricucci D, Siqueira JF. Biofilms and apical periodontitis: study of prevalence and association with clinical and histopathologic findings. *J Endod.* 2010;36(8):1277–1288.
6. George S, Kishen A, Song KP. The role of environmental changes on monospecies biofilm formation on root canal wall by Enterococcus faecalis. *J Endod.* 2005;31(12):867–872.
7. Love RM. Enterococcus faecalis – a mechanism for its role in endodontic failure. *Int Endod J.* 2001;34(5):399–405.
8. Shrestha A, Fong SW, Khoo BC, Kishen A. Delivery of antibacterial nanoparticles into dentinal tubules using high-intensity focused ultrasound. *J Endod.* 2009;35(7):1028–1033.
9. Besinis A, van Noort R, Martin N. Infiltration of demineralized dentin with silica and hydroxyapatite nanoparticles. *Dent Mater.* 2012; 28(9):1012–1023.
10. Fan W, Wu CT, Han PP, Zhou YH, Xiao Y. Porous Ca-Si-based nanospheres: a potential intra-canal disinfectant-carrier for infected canal treatment. *Mater Lett*. 2012;81:16–19.
11. Vallet-Regí M, Balas F, Arcos D. Mesoporous materials for drug delivery. *Angew Chem Int Ed Engl*. 2007;46(40):7548–7558.
12. Wang X, Li X, Ito A, Sogo Y. Synthesis and characterization of hierarchically macroporous and mesoporous CaO-MO-SiO(2)-P(2) O(5) (M=Mg, Zn, Sr) bioactive glass scaffolds. *Acta Biomater.* 2011; 7(10):3638–3644.
13. Wu C, Chang J, Fan W. Bioactive mesoporous calcium-silicate nanoparticles with excellent mineralization ability, osteostimulation, drug-delivery and antibacterial properties for filling apex roots of teeth. *J Mater Chem*. 2012;22:16801–16809.
14. Li X, Shi J, Zhu Y, et al. A template route to the preparation of mesoporous amorphous calcium silicate with high in vitro bone-forming bioactivity. *J Biomed Mater Res B Appl Biomater.* 2007;83(2):431–439.
15. Stewart GT, Coles HM, Nixon HH, Holt RJ. "Penbritin": an oral penicillin with broad-spectrum activity. *Br Med J*. 1961;2(5246):200–206.
16. Campoccia D, Montanaro L, Speziale P, Arciola CR. Antibiotic-loaded biomaterials and the risks for the spread of antibiotic resistance following their prophylactic and therapeutic clinical use. *Biomaterials.* 2010;31(25):6363–6377.
17. Rai MK, Deshmukh SD, Ingle AP, Gade AK. Silver nanoparticles: the powerful nanoweapon against multidrug-resistant bacteria. *J Appl Microbiol.* 2012;112(5):841–852.

18. Arciola CR, Baldassarri L, Campoccia D, et al. Strong biofilm production, antibiotic multi-resistance and high gelE expression in epidemic clones of Enterococcus faecalis from orthopaedic implant infections. *Biomaterials*. 2008;29(5):580–586.
19. Rai M, Yadav A, Gade A. Silver nanoparticles as a new generation of antimicrobials. *Biotechnol Adv*. 2009;27(1):76–83.
20. Jia H, Hou W, Wei L, Xu B, Liu X. The structures and antibacterial properties of nano-SiO_2 supported silver/zinc-silver materials. *Dent Mater*. 2008;24(2):244–249.
21. Chatzistavrou X, Fenno JC, Faulk D, et al. Fabrication and characterization of bioactive and antibacterial composites for dental applications. *Acta Biomater*. 2014;10(8):3723–3732.
22. Liong M, France B, Bradley KA, Zink JI. Antimicrobial activity of silver nanocrystals encapsulated in mesoporous silica nanoparticles. *Adv Mater*. 2009;21(17):1684–1689.
23. Armelao L, Bottaro G, Campostrini R, et al. Synthesis and structural evolution of mesoporous silica-silver nanocomposites. *Nanotechnology*. 2007;18(15):155606.
24. El-Kady AM, Ali AF, Rizk RA, Ahmed MM. Synthesis, characterization and microbiological response of silver doped bioactive glass nanoparticles. *Ceram Int*. 2012;38(1):177–188.
25. Shruti S, Salinas AJ, Lusvardi G, Malavasi G, Menabue L, Vallet-Regi M. Mesoporous bioactive scaffolds prepared with cerium-, gallium- and zinc-containing glasses. *Acta Biomater*. 2013;9(1):4836–4844.
26. Mohammadi G, Valizadeh H, Barzegar-Jalali M, et al. Development of azithromycin-PLGA nanoparticles: physicochemical characterization and antibacterial effect against Salmonella typhi. *Colloids Surf B Biointerfaces*. 2010;80(1):34–39.
27. Matsuo T, Shirakami T, Ozaki K, Nakanishi T, Yumoto H, Ebisu S. An immunohistological study of the localization of bacteria invading root pulpal walls of teeth with periapical lesions. *J Endod*. 2003;29(3):194–200.
28. Peters LB, Wesselink PR, Buijs JF, van Winkelhoff AJ. Viable bacteria in root dentinal tubules of teeth with apical periodontitis. *J Endod*. 2001;27(2):76–81.
29. Vieira AR, Siqueira JF, Ricucci D, Lopes WS. Dentinal tubule infection as the cause of recurrent disease and late endodontic treatment failure: a case report. *J Endod*. 2012;38(2):250–254.
30. Stuart CH, Schwartz SA, Beeson TJ, Owatz CB. Enterococcus faecalis: its role in root canal treatment failure and current concepts in retreatment. *J Endod*. 2006;32(2):93–98.